ROYAL SOCIETY OF CHEMISTRY

PAPER

Check for updates

CLiB – a novel cardiolipin-binder isolated *via* data-driven and *in vitro* screening†

Isabel Kleinwächter,[a] Bernadette Mohr,[b] Aljoscha Joppe,[c] Nadja Hellmann,[a] Tristan Bereau, [iD][b] Heinz D. Osiewacz[c] and Dirk Schneider [iD] *[ad]

Cardiolipin, the mitochondria marker lipid, is crucially involved in stabilizing the inner mitochondrial membrane and is vital for the activity of mitochondrial proteins and protein complexes. Directly targeting cardiolipin by a chemical-biology approach and thereby altering the cellular concentration of "available" cardiolipin eventually allows to systematically study the dependence of cellular processes on cardiolipin availability. In the present study, physics-based coarse-grained free energy calculations allowed us to identify the physical and chemical properties indicative of cardiolipin selectivity and to apply these to screen a compound database for putative cardiolipin-binders. The membrane binding properties of the 22 most promising molecules identified in the *in silico* approach were screened *in vitro*, using model membrane systems finally resulting in the identification of a single molecule, CLiB (CardioLipin-Binder). CLiB clearly affects respiration of cardiolipin-containing intact bacterial cells as well as of isolated mitochondria. Thus, the structure and function of mitochondrial membranes and membrane proteins might be (indirectly) targeted and controlled by CLiB for basic research and, potentially, also for therapeutic purposes.

Introduction

Cellular membranes separate intracellular processes from the environment and surround defined intracellular structures within cells, resulting in formation of defined intracellular reaction compartments, the organelles, a basis for the evolution of complex life.[1,2] Biomembranes consist of a scaffold of multiple membrane lipids, albeit the concentration of membrane-attached and/or integrated protein can be high. Biological membranes can contain more than 1000 different lipid species, where the main membrane constituents belong to three classes of lipids: phospholipids, glycolipids and cholesterol, with glycerophospholipids being the major class.[2,3] The exact lipid composition varies significantly between the diverse intracellular membrane systems in eukaryotes, with the membrane lipid composition of organelles differing from each

other as well as from the composition of the plasma membrane.[3] Eukaryotic membranes are typically asymmetric, with the lipid composition of an inner membrane leaflet differing from that of the outer.[2] *E.g.*, in highly curved membrane regions, such as the cristae of the inner mitochondrial membranes, the phospholipid cardiolipin (CL) is enriched in the inner membrane leaflet as it promotes and/or stabilizes negative membrane curvature.[4] Even within a lipid bilayer, regions with diverse lipid compositions can co-exist, such as the basolateral and apical regions of epithelial plasma membranes, and in eu- as well as in prokaryotes the formation of defined lipid domains is discussed, regions where distinct lipid species segregate. It is assumed that specific proteins diffuse into such domains and thereby form signalling platforms. (Targeted) disturbance of such lipid domains can severely affect cellular functions, resulting in mis-signaling.[5]

While the relative concentrations of individual lipid species within the eukaryotic membrane systems varies, and thus the exact lipid composition appears to define the membranes' physico-chemical properties, several lipids are restricted to chloroplasts and mitochondria, the organelles with an endosymbiotic origin. *e.g.*, galactolipids are solely found in chloroplasts, as expected due to their cyanobacterial origin.[6] Many bacteria contain significant amounts of CL (around 10% in *E. coli*),[5] whereas in eukaryotes this "bacterial lipid" can only be found in significant amounts in mitochondria.[7,8] In the inner membrane of mitochondria, CL typically constitutes 10–20% of

[a] Department of Chemistry, Biochemistry, Johannes Gutenberg University Mainz, Hanns-Dieter-Hüsch-Weg 17, 55128 Mainz, Germany.
E-mail: Dirk.Schneider@uni-mainz.de

[b] Van 't Hoff Institute for Molecular Sciences and Informatics Institute, University of Amsterdam, Amsterdam, The Netherlands

[c] Institute for Molecular Biosciences, J. W. Goethe University, Frankfurt am Main, Germany

[d] Institute of Molecular Physiology, Johannes Gutenberg University Mainz, Hanns-Dieter-Hüsch-Weg 17, 55128 Mainz, Germany

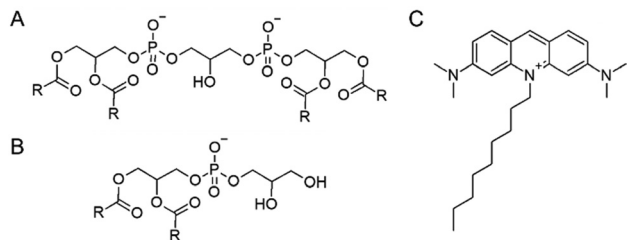† Electronic supplementary information (ESI) available. See DOI: https://doi.org/10.1039/d2cb00125j

© 2022 The Author(s). Published by the Royal Society of Chemistry

RSC Chem. Biol., 2022, **3**, 941–954 | 941

Fig. 1 Molecular structures of (A) CL, (B) PG and (C) NAO. In (A) and (B), R represents the fatty acid chains.

the total lipid,[9,10] whereas in the outer mitochondrial membrane only minor amounts of CL are found.[11,12] Consequently, CL is a marker for the mitochondrial inner membrane. In contrast, in fungi the CL content in mitochondria can be much lower,[13–15] and especially in mitochondria from *P. anserina* the CL level is very low (1.5%).[16]

Besides its unique origin and subcellular localization, also the structure of CL is uncommon (Fig. 1): two phosphatidyl backbones are linked *via* a glycerol head group, and thus one CL molecule contains two negative charges.[8,17,18] Four fatty acid chains are attached to this backbone, which typically differ in their respective length and saturation.[8,19,20]

Because of its overall cone-shaped structure, CL is primarily found in high curvature membrane regions, for example at the poles of rod-shaped bacteria[21,22] or at highly-curved regions of the mitochondrial inner membrane.[8] Consequently, alterations in the mitochondrial CL content can result in an altered morphology of the mitochondrial inner membrane.[23] Mitochondria are the dominant producer of adenosine triphosphate (ATP) in most eukaryotic cells and crucially involved in several metabolic processes.[8] CL is essential for the activity of several mitochondrial enzymes,[8,19] such as the glycerol-3-phosphate dehydrogenase,[24] creatine kinase or phosphate carriers,[25,26] and the activity of the respiratory chain complexes depends to some extent on CL.[19] Additionally, during apoptosis, interaction of CL with cytochrome *c* appears to trigger intracellular signal propagation.[27,28] Accordingly, CL deficiency or alterations in the mitochondrial CL levels have pathophysiological consequences in humans, such as ischemia or reperfusion, and result in diabetes, heart disease or the Barth Syndrome.[19,23,29] All these observations indicate that molecular engineering of drugs that target CL is an innovative chemical concept that potentially allows controlled analysis of physiological consequences caused by CL abnormalities. In general, when a membrane-active compound binds a defined lipid and/or affects lipid heterogeneity, this can (indirectly) affect the activity of proteins or protein networks that need the specific lipid and/or lipid-containing membrane-platforms to perform their cellular functions.[19] Based on this concept, the structure and function of mitochondrial membrane proteins might be indirectly controlled for basic research and, potentially, also for therapeutic purposes using engineered, CL-binding drugs ("CL-binders").

Presently, molecules that specifically bind CL are still rare. The antibiotic Daptomycin appears to bind more specifically to

CL than to the glycerophospholipid phosphatidylcholine (PC), yet with even higher affinity to phosphatidylglycerol (PG).[30] TTAPE-Me has been introduced as a promising candidate for binding CL,[31] yet here binding also appears to be rather non-specific.[32] Similarly, the synthetic tetrapeptide SS-31 binds to CL *via* hydrophobic and electrostatic interactions, yet it has been shown that it also interacts with phosphatidylserine (PS).[33]

10-*N*-Nonylacridine orange (NAO) (Fig. 1) has already been introduced decades ago as a mitochondrial surface marker, as it was suggested to specifically interact with CL.[34]

NAO intercalates into the inner mitochondrial membrane in a membrane potential independent manner and thereby poisons mitochondrial respiration.[35] At low concentrations, it inhibits ATP synthesis and at increased concentrations it additionally inhibits the respiratory electron transfer, potentially *via* competitively capturing CL.[34] In line with this, at high doses, NAO alters the structure of mitochondrial membranes.[36,37] The positively charged NAO likely electrostatically interacts with the negatively charged CL head group, and the CL fatty acid composition appears not to affect this binding specificity.[38,39] Upon CL-binding, a shift in the NAO fluorescence emission spectrum is observed. NAO is able to diffuse spontaneously across membranes, and can thus be well used *in situ*, in whole cells.[38] Consequently, NAO is used to visualize and quantify the CL content of and/or clustering within bacterial cells and/or mitochondria. Nevertheless, while a CL specificity has been postulated many times, it has turned out in recent years that NAO is not CL-specific. In fact, NAO still properly accumulates in mitochondria in CL-deficient yeast mutants,[40] and using model membranes it has been shown that NAO binds with high affinity to PG, which is chemically similar to CL (Fig. 1A and B). In summary, CL-selective molecules are urgently needed for future research.

In the present study, we set up an efficient pipeline to screen for novel specific CL-binders. Computational screening methods are gaining increasing recognition in materials modelling and drug design for efficient identification of molecular candidates that feature desired properties.[41] A microscopic picture not only provides the means to resolve the main physicochemical interactions at play, it can also directly connect chemical structure with property.[42] This connection allows the identification of a number of candidate molecules with structural features linked to desired properties that can be investigated in more detail. Molecular dynamics (MD) simulations can provide microscopic insight into macromolecular structure-property relationships that are difficult to gain experimentally.[43] Unfortunately, atomistic simulations remain prohibitive in the context of compound screening and rational design. Instead, we turned to coarse-grained (CG) models. Coarse-graining reduces the complexity of molecular representations by averaging over the chemical and physical properties of adjacent heavy (non-hydrogen) atoms represented by a single bead. The result is a considerable reduction in computational complexity, while still reproducing the underlying chemical and physical properties sufficiently well.[44–47] Here we show

that CG modelling is an efficient strategy to discover CL-binding small molecules (SM). Starting from the reference compound NAO, we employ a series of CG free-energy calculations to unravel the physicochemical interactions that lead to specific binding to CL. Free energy calculations *via* alchemical transformations explicitly compare differences in stability between CL and phosphatidylglycerol (PG) membranes. The calculations lead to the establishment of physicochemical design rules. In a separate study, we employed a more elaborate combination of CG simulations, free-energy calculations, deep representation learning, and Bayesian optimization to tackle the same CL-binding small-molecule discovery problem.[48] The results of this parallel study provide a more detailed description of the chemical space of putative CL-binders yet resulted in consistent physicochemical design rules. We subsequently applied these design rules to identify *via* computational screening 22 small molecules which potentially bind CL with high specificity. Subsequent *in vitro* analyses of these small molecules, using model membranes, resulted in the identification of a single molecule, CLiB (CardioLipin-Binder) with a high preference for CL over PG. *In vivo* analyses indicate that interaction of CLiB with CL affects respiration in bacteria as well as in mitochondria. Thus, we here introduce CLiB as a new chemical biology tool for studying the physiological role of CL in cells and/or organelles.

Results and discussion

Typically, the impact of CL on the physiology of mitochondria is analyzed in organisms or isolated mitochondria using strains in which CL synthesis is inhibited due to deletion of genes coding for CL-synthesizing enzymes. Yet, it remains an open question as to how far any physiological consequences observed in such deletion strains *de facto* reflect CL-dependent processes or are due to an altered membrane, the composition of which has been adjusted in the organisms when CL is absent. Thus, it clearly is desirable to manipulate the cellular CL content in a more controlled way using a chemical biology approach.

CL, the mitochondrial marker lipid, is crucially involved in stabilization of the inner mitochondrial membrane as well as in the stabilization and activity of mitochondrial proteins and protein complexes. Furthermore, the CL content of mitochondria is altered during cellular adaptation to defined stress conditions, as well as during aging.[11,49] Directly targeting CL by a chemical biology approach and thereby altering the cellular concentration of "free" CL eventually allows to systematically study the dependence of mitochondrial processes on CL availability. Therefore, we aimed at identifying a previously unrecognized small molecule that interacts specifically with CL and can be used in future research on mitochondrial physiology. To do so, we set up a workflow involving two initial computational steps, (i) the identification of physical and chemical properties crucial for CL selectivity of a small molecule and (ii) screening of a vendor database for possible candidates. This was done by applying a physics-based CG model of a known CL probe, reducing the complexity of chemical space, and thereby allowing us to systematically observe the change in selectivity caused by the introduction of new interaction types into the CG model. The observations were formulated as design rules describing which substructures in candidate molecules are indicative of the properties required for CL selectivity. The pre-selected candidate molecules were subsequently *in vitro* screened to identify promising candidate substances. Finally, the activity of the top CL-binders identified in the present study on the physiology of a CL-containing bacterium as well as on mitochondria was evaluated.

Rational identification of 22 candidate molecules with a putative CL-binding propensity

Due to its claimed CL-selectivity, NAO is commonly used to stain CL-containing membranes, or CL-containing membrane domains. Yet, its specificity and sensitivity towards CL is not high (as often proposed), as it also interacts with other negatively charged lipids, such as PG, phosphatidylserine (PS) and phosphatidylinositol (PI).[35,50] Nevertheless, the chemical structure of NAO can serve as a reasonable starting point to search for new CL-binders. Our approach then consisted of locally probing chemical space to identify more selective compounds. The underlying assumption was the presence of local regions of chemical space, or basins, that offer high selectivity—a hypothesis that we checked in a recent publication.[48]

Via free-energy calculations, and in particular alchemical transformations, changes in chemical interactions were directly linked to selectivity improvements. The physical and chemical properties of the CG representation of NAO were systematically varied by exchanging individual bead types, for instance by altering the number of hydrophobic sites or charged groups and calculating the relative partitioning free energy $\Delta\Delta G$ of the altered CG NAO from the water phase into each lipid membrane. This is accomplished through two different free-energy methods, performing alchemical transformations[51–53] and calculating the potential of mean force (PMF), see Fig. 8B. Negative $\Delta\Delta G$ and minima of the PMF curve represent energetically favorable processes, *i.e.*, insertion at the membrane-water interface and selectivity to the targeted CL. We monitored the influence of the bead-type exchanges on the preferential stability for CL compared to PG. The resulting partitioning free energy differences $\Delta\Delta G_{PG \to CL} = \Delta\Delta G_{CL} - \Delta\Delta G_{PG}$ between the same bead-type transformation in both the CL membrane and the PG membrane are shown in (Fig. 2A). The modified NAO structures are represented on the horizontal axis, the color code indicates the position in the CG structure a specific bead was assigned to (Fig. 2B). Due to the symmetry of the reference NAO structure along its vertical axis, for the pink and blue bead positions, no distinction was made whether a specific bead was placed on the left or on the right side of the molecule.
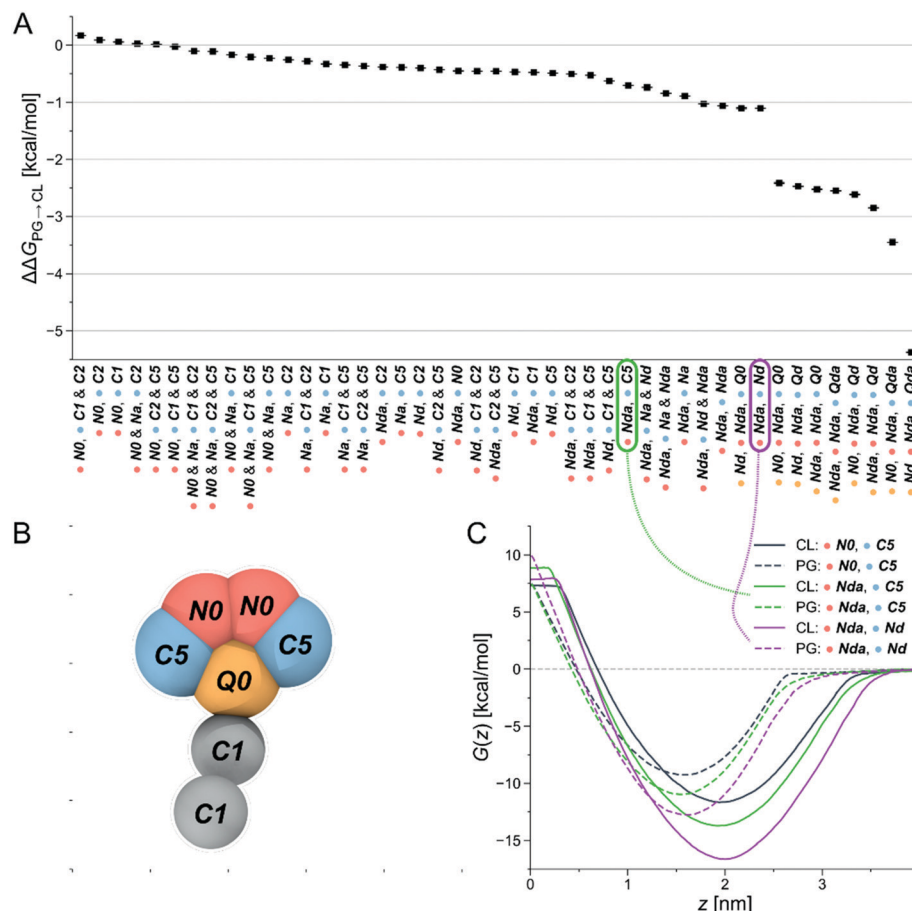
© 2022 The Author(s). Published by the Royal Society of Chemistry

RSC Chem. Biol., 2022, **3**, 941–954 | **943**

Fig. 2 Computational selection of SM$_{1-22}$. (A) Differences in partitioning free energies $\Delta\Delta G_{PG\to CL}$ from alchemical transformations of one or more beads in the CG-representation of NAO. (B) Original CG representation of NAO color-coded to visualize the locations of bead changes in the free energy calculations. (C) Exemplary PMFs of CG structures with different bead types in the CL membrane (solid lines) and the PG membrane (dashed lines). Connections show which PMF curve corresponds to which partitioning free energy difference $\Delta\Delta G_{PG\to CL}$.

The CL-selectivity $\Delta\Delta G_{PG\to CL}$ is represented on the y-axis. The compounds are sorted by their resulting $\Delta\Delta G_{PG\to CL}$, from left (low selectivity) to right (high selectivity). The Martini coarse-grained force field[56] defines 14 neutral bead types sorted by increasing polarity, from C1–C5 (very apolar) *via* N-types (neutral) to P-types (polar). Additionally, it provides four charged bead types (*Q*). From here on, we denote all CG Martini bead types in **bold** and *italics*. It becomes clear that increased hydrophobicity brought on by replacing the two **C5** beads on the outer sides of the original CG NAO structure (blue) by **C1** or **C2** beads shifted the selectivity of the resulting CG structure away from CL and towards PG ($\Delta\Delta G_{PG\to CL} > 0$). Adding a neutral **Na** bead with hydrogen-bond acceptor properties instead of the original **N0** beads to the top of the structure (pink) had no noticeable effect on CL-selectivity. In contrast, introducing hydrogen-bond donor properties to the pink beads (**Nda/Nd**) together with weak hydrophobicity (**C5**) in the blue beads resulted in an increase in CL-selectivity. This trend was increased further by replacing the hydrophobic **C**-types at the blue positions with neutral beads with added hydrogen-bond donor sites (**Nda/Nd**). Finally, the biggest increase in CL-selectivity was obtained in the calculations by replacing the

central charged bead (yellow) with a neutral hydrogen-bond donor bead type, keeping the same bead types at the pink bead positions, and introducing two positively charged hydrogen-bond donor beads (**Qd/Qda**) at the blue positions on the outside of the molecule.

In summary, slightly shifting the overall hydrophobicity of the CG NAO representation towards a more amphiphilic character, adding hydrogen bond donor properties, and doubling the positive charge while simultaneously moving the charged beads from the center to the outsides of the CG structure led to a larger negative $\Delta\Delta G_{PG\to CL}$, indicating increased CL selectivity. These design rules can be directly translated to binder-lipid intermolecular interactions: electrostatics with the phosphate group of the lipid head, and amphiphilic character to anchor the compound at the water-membrane interface. Example PMFs for three of those molecules are shown in Fig. 2C. Here, the solid lines represent PMFs calculated in the CL membrane, the dashed lines PMFs in the PG membrane. The grey PMF curve resulted from the original NAO representation to provide a reference for our introduced bead-type changes. The purple and the green lines represent the bead-type conformations circled in the same colors in Fig. 2A. The increased depths of

the minima of the PMF curves indicate an increased selectivity of the candidate compounds for both the PG and the CL membranes, and the increased distance at the minima of the PMF curves for the same compound indicate an increased selectivity for CL over PG. Overall, the umbrella sampling results show the same trend as found in the alchemical transformation results shown in Fig. 2A. Due to the increase in computational cost, umbrella sampling calculations with more than one charged bead were not performed.

Our observations now allowed us to express three design rules of molecules that selectively bind to CL and prefer CL over PG:

1.Positively charged beads: at least one, ideally two sites that will carry a positive charge at physiological pH (pH ≈ 7.3).

2.Neutral and charged beads (N- and Q-types) with hydrogen-bond donor properties: Functional groups able to form hydrogen bonds with the CL headgroup.

3.Apolarity (represented by the C1 beads in the tail): Hydrophobic areas in the molecule that induce alignment with or insertion into the lipid bilayer.

Those findings are in good agreement with the interaction types described as being crucial in a comprehensive study on CL-binding proteins, where positively charged amino acids have been identified to be overrepresented in sites binding to the CL headgroup, and hydrophobic amino acids were dominant in sites binding the acyl chains.[57]

The design rules allowed us to select candidate molecules for CL selectivity from the MCULE database (Fig. 8C).[58] As NAO is described as a CL probe in the literature, the Tanimoto similarity coefficient[59,60] to NAO at the level of fingerprint representations of the molecules was used for comparison. Candidate molecules with a Tanimoto coefficient >0.39 (lower threshold for similarity, identity is 1.0) were extracted. We further screened the candidates for the presence of positively ionizable sites and aromaticity.[61] From the resulting

93 molecules, a subset of 16 candidates with a Tanimoto coefficient >0.44 were subjected to experimental validation (SM_1 to SM_7, SM_{10} to SM_{12}, SM_{16} and SM_{18} to SM_{22}). Eight of the 16 molecules had at least one hydrogen-bond acceptor site identified using the RDKit[62] chemical features definition, and one of those eight had both hydrogen-bond donor and acceptor sites. Six molecules with a lower Tanimoto coefficient were also added to cover the aspects of the design rules in more detail (SM_8, SM_9, SM_{13} to SM_{15} and SM_{17}). Only hydrogen-bond donor- and no acceptor sites were identified in SM_{13} to SM_{15}, SM_8 showed five positively ionizable sites, SM_9 four hydrogen-bond acceptor sites and one donor site. Additionally, SM_{14} and SM_{15} are structurally very similar to SM_{16}, even though their Tanimoto similarity to NAO is lower. SM_{17} follows the design rules, even though the similarity to NAO was lower than that of the 16 initially selected candidates. It was included to probe the role of the structural similarity to the detected CL selectivity. The 22 molecules are shown in Fig. 3, all descriptors used for their selection can be found in Table S1 in the ESI.†

We successfully applied a combination of physics-based coarse-grained representations of molecules to reduce the combinatorial complexity of chemical space together with efficient free-energy calculation methods, thereby greatly increasing the efficiency of examining the influence of different physical and chemical properties on our targeted CL selectivity. We were able to formulate design rules describing the identified properties on the CG level and linking back to related characteristics in molecular structures. The design rules were successfully used to screen the MCULE database of purchasable, in-stock compounds for potential CL-binders (Fig. 3).

Membrane binding properties of $SM_{1–22}$

The CG free energy calculations allowed us to identify the physical and chemical properties indicative of CL selectivity, to formulate design rules and to apply those to screen a
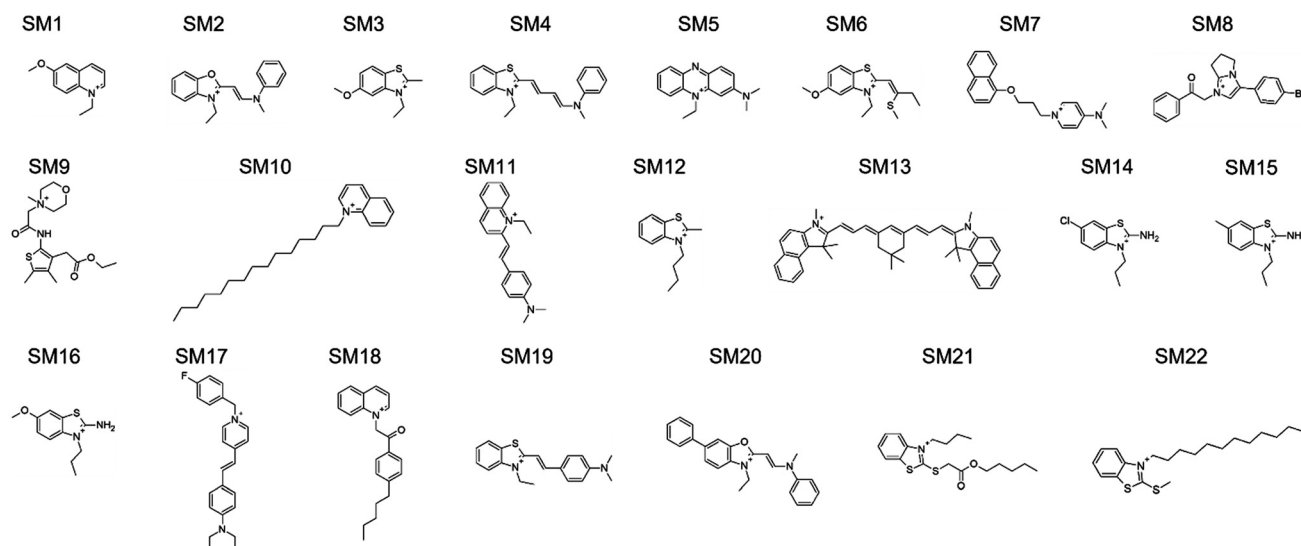

Fig. 3 Structures of 22 SMs selected *in silico* and further analyzed. The chemical names of the substances can be found in Table S2 in the ESI.†

database for candidate molecules conforming to those design rules. To experimentally verify our *in silico* results, we next screened the membrane binding properties of the 22 molecules identified in the *in silico* approach *in vitro*, using liposomal systems.

When a small molecule integrates into a hydrophobic lipid bilayer due to its amphipathic character, this will affect lateral lipid packing, an effect often observed *e.g.* with alcohols or other small, hydrophobic molecules.[63] Additional specific interactions with certain lipid headgroups will lead to an increase in the effective substance concentration at the surface of the bilayer, and therefore to an increased effective partitioning coefficient (see *e.g.* ref. 64). Furthermore, the effect on order and packing of the hydrophobic part might be altered, *e.g.* due to a different orientation of the small molecule when specifically binding to a defined lipid species. Thus, comparing the impact of a small molecule on the membrane structure in a system where the molecules merely partition into the membrane with a system where the molecules additionally (more or less) specifically interact with a defined lipid species will allow parallel screening of multiple molecules for their potential to bind to CL. We rationalized that the molecules preselected in the computational screen will "only" integrate into net uncharged pure phosphatidylcholine (PC) membranes but will (in the best of all cases) specifically interact with CL in CL-containing membranes. To distinguish general membrane partitioning from specific lipid binding, we additionally tested the structure of a model membrane system where PG is present to isolate selectivity to CL by direct comparison. For monitoring changes in the membrane lipid structure, we utilized Laurdan, an environment-sensitive fluorescent dye that incorporates into lipid bilayers. From the Laurdan fluorescence emission spectra the generalized polarization (GP) values were calculated (eqn (5))[65] for membranes in absence *vs.* presence of the 22 substances identified in our computational screening. Besides pure PC and the PG- or CL-containing PC membranes, respectively, we also monitored the Laurdan fluorescence emission in PC liposomes containing phosphatidylethanolamine (PE), another net-uncharged phospholipid. PE introduces membrane curvature stress, and these measurements enabled us to test whether any observed effects on the Laurdan fluorescence spectra were mainly due to changes in the lateral membrane pressure. This would result in changes observed in the PC/PE system being unequal to the pure PC system. The Laurdan GP value is largely independent of the lipid head group and its acyl chain chemistry, and therefore any changes of this value upon the addition of a substance provides information about changes in the lipid order.[66] Thus, if the GP value in presence of a substance is altered, one can infer that binding/incorporation of the substance has occurred. Indeed, for a number of substances large positive ΔGP values were observed (Fig. 4).

Addition of SM_4, SM_5, SM_{11}, SM_{13}, SM_{17} and SM_{19} resulted in substantial changes in the G_P values (high ΔGP values) in all lipid systems, which clearly indicates considerable interaction of these SMs with the membranes. Noteworthy, while we did
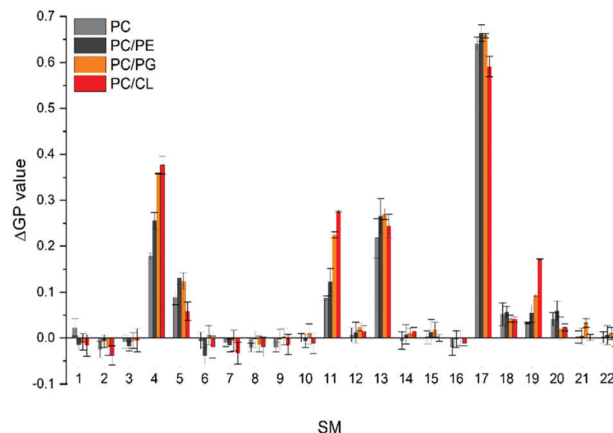

Fig. 4 ΔGP values determined in various model membrane systems in presence of the preselected 22 SMs. GP values were measured using pure PC liposomes, as well as liposomes containing PC/PG, PC/PE and PC/CL, all in a molar ratio of 80/20 (mol%/mol%) at 300 µM total lipid. Low ΔGP values indicate no influence of the respective SM on the membrane structure. The more a ΔGP value deviates from 0.0, the higher is the respective impact of a given SM on the membrane structure. Positive ΔGP values indicate a decreased polarity in the environment of Laurdan, as *e.g.* the case upon increased lipid ordering due to the presence of a SM within a membrane.

not observe ΔGP changes for the remaining SMs, this does not finally exclude that these SMs do interact with membranes. We only limited the selection and further analysis in the screening pipeline developed and presented here, to substances which had a measurable impact on membrane lipid packing, as sensed by Laurdan. While all six molecules affected the Laurdan fluorescence emission spectrum, for SM_5, SM_{13} and SM_{17} the results did not indicate a specificity towards charged lipids, as anticipated, as the ΔGP values were similarly affected in membranes containing solely zwitterionic or additionally negatively charged lipids. Thus, a specific interaction with negatively charged lipids is unlikely. In contrast, SM_4, SM_{11} and SM_{19} showed higher ΔGP values in CL- and PG-containing PC membranes, indicating a specificity towards negatively charged lipids.

The objective of our research was to identify membrane-active compounds with a putative specificity towards CL. Thus far, our initial computational and *in vitro* screens limited our further analyses to three compounds, for which we next analyzed in greater detail their respective impact on the GP values of CL-containing liposomes compared to PG-containing liposomes. The magnitude of a GP value change observed upon SM binding might be specific for the substance and the lipid environment. Yet, with increasing amounts of negatively charged lipids but at a constant SM concentration, the ΔGP values are affected more substantially when an observed change is due to a specific interaction of the substance with the lipid and thus information about the relative specificity can be extracted: a steeper relative increase of ΔGP values is an indicator for a higher affinity. Therefore, we next monitored how the G_P values determined in a (neutral) PC background are differentially affected when the mole fractions of the two
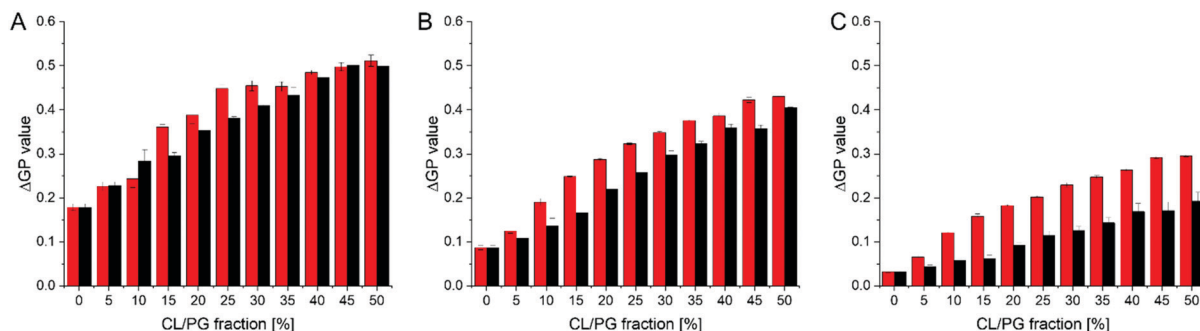
Fig. 5 ΔGP values in presence of the three most promising CL-binders determined in CL- or PG-containing model membranes. ΔGP values were determined in liposomes, containing increasing amounts of the negatively charged lipids PG (black) or CL (red), respectively, in a PC background (300 μM total lipid) at a constant concentration (3 μM) of SM_4 (A), SM_{11} (B) and SM_{19} (C). All SMs induce an increase in ΔGP values with increasing amounts of the negatively charged lipids. The most significant difference between PG- vs. CL- containing membranes was observed for SM_{19}.

negatively charged lipids PG or CL, respectively, increase (Fig. 5), yielding a binding isotherm. In presence of all three SMs, increasing ΔGP values were observed with increasing amounts of negatively charged membrane lipids. Yet, in case of SM_4 the shape of the relative increase is similar for CL- and PG-containing membranes, and also the ΔGP values are similar. Thus, SM_4 (Fig. 5A) does not significantly discriminate between liposomes containing PG or CL, indicating about similar interaction with the negatively charged membrane lipids. For SM_{11} (Fig. 5B), a difference between liposomes containing PG and those containing CL was observed at all PG/CL concentrations. Furthermore, the curve is slightly steeper at the initial part in case of CL, indicating a specificity of SM_{11} for CL. Finally, in case of SM_{19}, the ΔGP values are overall lower than for the other two substances, yet the difference in the values obtained for CL- vs. PG-containing liposomes is larger. More importantly, the binding isotherm is steeper in case of CL-containing liposomes. Thus, SM_{19} (Fig. 5C) clearly discriminates best between CL- or PG-containing liposomes. In order to visualize the differences in shape of the binding isotherms more clearly, the ratio between the ΔGP values obtained in presence of CL or PG, respectively, was calculated

(Fig. S3, ESI†). If the shapes of the binding isotherms were identical, yet differ in their ΔGP value, the same ratio (within error limits) is expected at all mole fractions of anionic lipids. The data obtained in presence of SM_{19} clearly show the largest deviation from a constant ratio, and thus, based on these analyses, SM_{19} has the highest specificity towards CL (compared to PG).

To obtain an estimate of the SM_{19} affinity for CL, changes in the membrane lipid order were monitored at a constant lipid- but at varying SM_{19} concentrations (Fig. 6A). The CL content in the liposomes was 10%, approximately mirroring the CL concentration in E. coli and mitochondrial membranes.[11] In agreement with the above presented results, addition of increasing amounts of SM_{19} lead to higher ΔGP values in case of CL-containing membranes when compared to PG-containing membranes. However, the shape of the curves does not allow to estimate the affinity constant. In agreement with the data in Fig. 4 and 5, the ΔGP value is consistently higher in case of CL compared to PG. As SM_{19} is intrinsically fluorescent (Fig. 6B, inlet), we next additionally analyzed SM_{19} interaction with negatively charged lipids via following the SM_{19} fluorescence. In both PG- as well as CL-containing PC liposomes, the
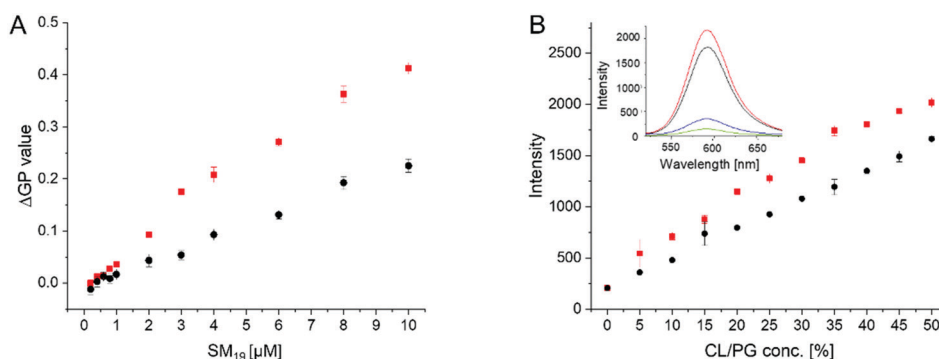

Fig. 6 Specificity of SM_{19}-binding to CL-containing PC membranes. ΔGP values determined in PG- or CL- containing model membranes in presence of increasing SM_{19} concentrations. ΔGP values were measured using liposomes containing a fixed lipid composition of 90% PC and 10% CL (red) or PG (black), respectively, at increasing amounts of SM_{19}. At low SM_{19} concentrations no significant differences were observed. (B) The inherent SM_{19} fluorescence properties are affected by the membrane lipid composition. The fluorescence emission at 592 nm increases with increasing fractions of negatively charged lipids (PC/PG (black), PC/CL (red)). The intensity increase is consistently higher in CL-containing membranes. (B inlet) Emission spectrum of pure SM_{19} in buffer (green), or in pure PC (blue), PC/PG (50/50) (black) and PC/CL (50/50) liposomes (red) (SM_{19} concentration: 3 μM).

© 2022 The Author(s). Published by the Royal Society of Chemistry

RSC Chem. Biol., 2022, 3, 941–954 | 947

intensity of the SM_{19} fluorescence is rising with increasing concentrations of negatively charged lipids, which is perfectly in line with the Laurdan measurements (Fig. 6A). Already when SM_{19} was added to pure PC liposomes, the fluorescence emission increased (Fig. 6B), indicating that membrane incorporation of SM_{19}, *i.e.*, placing the dye in a more hydrophobic environment, affects the SM_{19} fluorescence properties. When the liposome surface charge was increased *via* increasing the amount of PG or CL, respectively, the fluorescence emission intensity steadily increased. Thus, interaction of SM_{19} with negatively charged lipids can also be monitored *via* the substances' inherent fluorescent properties and, as observed before using Laurdan as a probe, this effect is more pronounced in CL-containing liposomes.

Impact of SM_{19} on CL-containing cellular membranes

In the above presented *in silico* and *in vitro* analyses, SM_{19} has emerged as the most promising CL-binder. Yet, as we aimed to establish SM_{19} as a chemical tool allowing to directly target CL-containing membranes in biological systems, we next tested the impact of SM_{19} on the respiration of bacterial (*E. coli*) cells as well as of isolated mitochondria (*P. anserina*).

Similar to mitochondria (10–20%), *E. coli* cells contain $\sim 10\%$ CL in their membrane as well as around 20% PG.[5] When SM_{19} was added to *E. coli* cells at increasing concentrations, the SM_{19} fluorescence emission intensity at 592 nm increased (ESI,† Fig. S1), indicating membrane incorporation. To next study the impact of a SM_{19}-induced CL tethering on the physiology of *E. coli* cells, the impact of SM_{19} addition on *E. coli* respiration was analyzed. In fact, SM_{19} addition significantly affected the respiration rates of *E. coli* cells. Without the substance the respiration rate was around -19 $\pm$ 0.7 µmol oxygen per min per L, which decreased in the presence of SM_{19} to -15 ± 0.5 µmol oxygen per min per L.

As these initial observations indicated a direct impact of SM_{19} on the activity of proteins embedded in CL-containing membranes, we then ultimately analyzed the impact of SM_{19} on mitochondrial respiration determined using mitochondria isolated from the fungus *P. anserina*. In presence of SM_{19}, the relative oxygen consumption was decreased by around 40% in wild type mitochondria (Fig. 7), indicating that SM_{19} efficiently tethers CL in mitochondrial membranes.

To finally test whether this impact of SM_{19} on mitochondrial respiration was due to a specific interaction of the compound with CL, we next used a CL-free *P. anserina* strain[16] and tested the impact of SM_{19} on mitochondrial oxygen consumption using CL-free mitochondria. While the respiration rate is already reduced in CL-free mitochondria, addition of SM_{19} showed only marginal effects. To also exclude that the non-responsiveness of CL-free mitochondria is due to their general impairment in respiration, we additionally tested whether they respond to inhibition of the two terminal oxidases present in *P. anserina*.[67] While complex IV (COX) is inhibited by KCN, SHAM inhibits the alternative oxidase AOX. Thus, mitochondrial respiration should be completely blocked when both inhibitors are given in combination. In fact, both in wild type
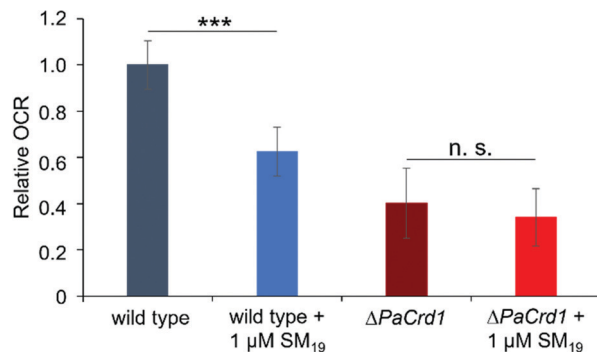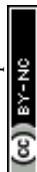

Fig. 7 Oxygen consumption measured with mitochondria isolated from 6 days old wild-type and ΔPaCrd1 isolates. Measurements were performed in absence *vs.* presence of 1 µM SM_{19}. Oxygen consumption rate (OCR) in the phosphorylating respiration state (in the presence of ADP) of the wild type was set to 1. In the wild-type, SM_{19} treatment significantly reduced phosphorylating respiration by 40% compared to the control. In contrast, in the mutant, addition of SM_{19} had only marginal effects. (Measurements of the phosphorylating respiration of wild type ($n = 15$), of wild type + 1 µM SM19 ($n = 8$), of ΔPaCrd1 ($n = 14$) and of ΔPaCrd1 + 1 µM SM19 ($n = 9$); mean values $\pm$ standard deviation are shown; significant differences are marked with "***", $p < 0.001$; n. s.: not significant).

and ΔPaCrd1 mitochondria the respiration rate was significantly decreased after addition of KCN/SHAM (Supplementary data, Fig. S2, ESI†). Thus, the non-responsiveness of ΔPaCrd1 to SM_{19} was indeed due to the lack of CL in this strain. These observations strongly indicate that SM_{19} specifically interacts with CL as the substance clearly has an impact on the oxygen consumption rates (OCR) in wild type but not in CL-free mitochondria.

SM_{19} clearly affects respiration of intact *E. coli* cells as well as of isolated *P. anserina* mitochondria. Importantly, a similar effect on respiration of CL-containing mitochondria was not observed with SM_{18}, again underlaying the specificity of SM_{19} (see Fig. S4, ESI†). As an impact of SM_{19} was not observed when CL-free mitochondria were analyzed, the observed effects on respiration were very likely caused by CL-tethering *via* SM_{19}.

Thus, after identifying 22 putative CL-binders *in silico* and further analyzing them *in vitro*, we finally identified a single small molecule, 2-[(E)-2-[4-(dimethylamino)phenyl]ethenyl]-3-ethyl-1,3-benzothiazol-3-ium iodide (SM_{19}) (Fig. 3), which interacts with negative charged lipids and prefers CL over PG. Therefore, we will from now on name this molecule CLiB (CardioLipin-Binder).

The interaction of CLiB with CL might be due to its quaternary ammonium ion (Fig. 1), an interaction known to drive binding of NAO to CL and PG.[38] As the lipid composition in bacteria and eukaryotic cells can substantially differ in the chemistry of the acyl chains,[68–72] the specificity of CLiB towards CL appears to be mainly based on the interaction with the lipid headgroup. While the structures of PG *vs.* CL are very similar (Fig. 1), the main difference is their respective charge. Thus, a specificity of a given substance would probably be based on a change in entropy: binding to a single CL molecule might be thermodynamically more favorable than binding two PG

948 | *RSC Chem. Biol.*, 2022, **3**, 941–954

© 2022 The Author(s). Published by the Royal Society of Chemistry

molecules due to a reduced loss in entropy. This is reflected in the design rules calling for two positively charged sites in the candidate structures to increase selectivity. The two positive charges correspond to the two negatively charged phosphate groups present in a CL molecule. Yet, this effect is likely very small, and thus it is potentially a deleterious task trying to isolate a substance with 100% specificity towards CL.

In summary, we have identified and introduce here CLiB, a novel small molecule able to bind to negatively charged phospholipids, with a clear preference for CL (over PG). However, incorporating CLiB into a membrane and CL-binding could have unspecific toxic effects on a living organism, for example due to the induced change in the membrane structure caused by the interaction between CLiB and CL (see Fig. 4). Yet, CLiB now allows to systematically analyze the role of CL in biological membranes and in membrane-harbored physiological processes, at least *in vitro*, as with this chemical biology tool CL can be specifically targeted. We are optimistic that the identification of CLiB will now trigger new analyses of mitochondrial processes, involving aging and dysfunction.

Conclusions

To find a drug/molecule that specifically targets CL, potentially allows controlled analysis of physiological consequences caused by CL abnormalities. So far, such specific CL-binders are rare. For this reason, we set up an efficient pipeline to screen for novel cardiolipin-binders. Starting with CG free-energy calculation and computational screening methods, followed by *in vitro* and finally some *in vivo* studies, we discovered a molecule, showing a clear preference for binding to cardiolipin. This workflow and especially the *in silico* screening can, in our specific use-case, be applied to other databases and lead to the identification of possibly more specific CL binders. Furthermore, we thus far limited our search for natural compounds. Yet, the here identified design principles might even serve to design a novel molecule with increased CL-binding propensity. Finally, the method of identifying design rules can also be generalized to discover candidate small molecules with a high binding affinity to any given molecular target.

Experimental section

Chemicals

All lipids were purchased at Avanti Polar Lipids (Alabaster, ALA, US). The substances 1–22 (further described in the text) were purchased at MCULE (Budapest, HUN). All other chemicals were purchased at Sigma Aldrich (Munich, GER). Structures were drawn with the program ChemSketch V5 (Freeware from ACD/Labs, Toronto, Ontario, Canada).

Molecular representations

Coarse-grained (CG) representations of each lipid from the Martini 2 force field were used.[56] The bead types defined in the Martini force field link to specific physicochemical
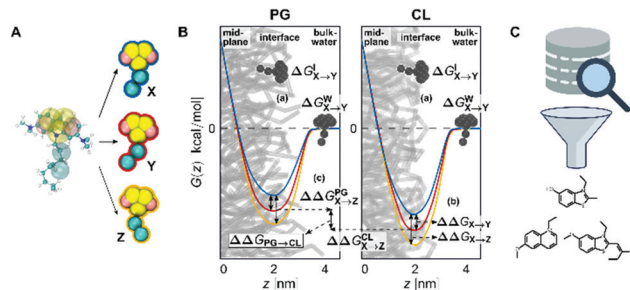

Fig. 8 The computational workflow. (A) Introduction of new chemical interactions by systematically changing of individual bead types. (B) The different areas of a membrane system where free energies are calculated. The black compounds indicate the two regions for the alchemical transformations, the PMFs show the free energy change of a molecule moving along the membrane normal z. The deeper the minimum of the PMF at the interface, the more selective the candidate is for the lipid headgroup. (C) Screening of a database of small molecules for candidates conforming to our identified design rules. The structures were drawn using RDKit (Landrum), the images were obtained from https://Flaticon.com.

interaction types, considering four main types of interactions: polar (P), nonpolar (N), apolar (C), and charged (Q). Within a main type, subtypes are distinguished either for hydrogen-bonding capability (d ≡ donor, a ≡ acceptor, da ≡ both, 0 ≡ none) or by a number indicating the degree of hydrophobicity (from 1 ≡ strongly hydrophobic to 5 ≡ weakly hydrophobic).[73] CL was modelled from dianionic tetraoleoyl-cardiolipin (TOCL).[74–76] We chose the Cardiolipin (CL) representation carrying two negative charges, following evidence of CL likely being fully ionized at physiological conditions.[7,17,18] The CG force field of PG represents 1-palmitoyl-2-oleoyl-*sn*-glycero-3-phosphoglycerol (POPG). While bilayers consisting of only one lipid type are not found in nature, we used homogeneous membranes as proxy systems to isolate the contributions of individual lipid types to the investigated interactions. Homogeneous bilayers for each lipid were created using the CHARMM-GUI Martini Maker[77] with the Martini[56] force field version 2.0, 06/2015. We solvated the membranes with the Martini polarizable water.[78] The net charges of the systems were brought to zero by adding the appropriate number of negatively charged counter ions per head group (one ion for PG, two for CL). This led to the CL simulation system containing 98 lipid representations (49 per membrane leaflet), 3609 water particles, and 196 counter ions. The PG system contained 118 lipids, 1957 water particles and 118 counter ions. The CG force field of NAO was generated using the auto-martini algorithm[79] and then manually refined to balance the overestimated hydrophobicity of the aromatic groups. Subsequently, new chemical interactions were introduced by systematically changing individual bead types and monitoring the resulting change in free energy (Fig. 8A).

Molecular dynamics (MD) simulations

MD simulations were performed in Gromacs 5.1.[80] The integration time step was $\delta t = 0.02\tau$, where τ is the time constant defined as $\tau = L\sqrt{M/E}$ with the units of length L, mass M and energy E. Temperature and pressure of the system ($T = 300$ κ and $P = 1$ bar) were controlled by means of a velocity rescaling

thermostat[81] and a Parrinello–Rahman barostat,[82] with coupling constants $\tau_T = \tau$ and $\tau_P = 12\tau$. Long-range electrostatic interactions were calculated using Particle-mesh Ewald summation.[83] Other parameters, such as cut-off range and dielectric constant, follow recommendations for the Martini force field.[84] The small molecule was inserted at the appropriate position in the system, either at the membrane–water interface or in the water phase (see Fig. 8B). The whole system was subsequently minimized and equilibrated for 8 ns. The free energy calculations were performed in a production run for 40 ns following the protocol described below.

Free-energy calculations

A change in free energy ΔG between two states of a system indicates whether the transitioning process between those states is thermodynamically favorable ($\Delta G < 0$) or not ($\Delta G > 0$). We compared the difference in partitioning free energies of different NAO-derived CG candidates into a CL membrane and a PG membrane at the interface region (Fig. 8B). Thereby, we identified which types of physicochemical interaction introduced into the CG candidate structures positively influence CL selectivity. This is measured as the difference in partitioning free energy of a candidate compound between the two different lipid membranes, $\Delta\Delta G_{PG \to CL}$ (Fig. 8B(c)).

The free energy change was calculated by two different methods; by the transformation of a parameter of the potential energy function (alchemical transformations[61–63]) or as a potential of mean force (PMF) along a reaction coordinate defined on atomic coordinates shown as red, blue and yellow curves in Fig. 8B) (umbrella sampling[54,55]).

We used the less computationally expensive alchemical transformation approach for an initial screening, the promising compounds were validated using umbrella sampling.

Alchemical transformations

Alchemical transformations[51–53] allow us to estimate the free-energy difference of physical processes by transforming an initial state A of a molecular system to an end state B *via* a succession of intermediate steps. This facilitates the calculation of free energy differences between states not necessarily connected by actual chemical or physical processes. Using this method, we were able to determine the influence of introducing different chemical interactions by turning individual CG beads from one bead type into another. State A is the free energy calculated for the CG representation of the original NAO molecule; state B is the corresponding free energy for a modified version of NAO. The transformation free energy was calculated by defining a thermodynamic path between the states and integrating over the ensemble average of the potential energy changes relative to a coupling parameter λ along this path (eqn (1)).

$$U(\lambda) = U_X + \lambda(U_Y - U_X) \tag{1}$$

$$\Delta G_{X \to Y} = \int_0^1 d\lambda \left\langle \frac{\delta U(\lambda)}{\delta\lambda} \right\rangle_\lambda \tag{2}$$

To investigate the influence of van der Waals interactions modeled by the Lennard-Jones potential (LJ), 20 intermediate steps between state A and state B were calculated with successively increasing values for $\lambda \in [0, 1]$. The influence of electrostatic interactions was evaluated by introducing additional charged particles or moving the position of existing charges involved. The interactions of charged beads were transformed first through 18 LJ steps followed by 18 Coulomb steps, adding up to 36 intermediate steps. The net charge of the system was kept at zero by simultaneously transforming the appropriate number of ions in the solution into water particles.[85,86] The individual free energy contributions of the intermediate steps were integrated into the overall free energy change ΔG between states X and Y using the MBAR method,[87,88] which also gives the statistical uncertainty of the calculated free energy.

We calculated the transfer free energy $\Delta G_{W \to I}$ of a candidate compound from bulk water to the membrane interface to determine whether this compound freely partitions into the membrane. This partitioning free energy $\Delta G_{W \to I}$ comprises the transformation free energy (eqn (2)) $\Delta G_{X \to Y}^I$ of this compound at the interface region and the transformation free energy $\Delta G_{X \to Y}^W$ of the same compound in the bulk water phase, following eqn (3):

$$\Delta G_{W \to I} = \Delta G_{X \to Y}^I - \Delta G_{X \to Y}^W = (\Delta G_Y^I - \Delta G_X^I) - (\Delta G_Y^W - \Delta G_X^W) \tag{3}$$

This necessitated three individual series of calculations for each NAO variant, one at the interface of each membrane and one in bulk water (Fig. 8B(a)). To keep the small molecules in the interface region of the membrane-containing systems, a small constraint force of 500 kJ mol^{-1} nm^{-2} was applied.

To evaluate the selectivity of the modified NAO structures for CL over PG, we used the free energy difference $\Delta\Delta G_{PG \to CL}$ (eqn (4)) between the partitioning free energies of the candidate compounds into each membrane

$$\Delta\Delta G_{PG \to CL} = \Delta G_{W \to I}^{CL} - \Delta G_{W \to I}^{PG} \tag{4}$$

$\Delta\Delta G < 0$ indicated that the modified NAO representation binds more selectively to CL than to PG (Fig. 8B(c)).

Umbrella sampling

Umbrella sampling[54,55] is a free-energy technique that allows the calculation of the potential of mean force (PMF) from moving a molecule along defined reaction coordinates (Fig. 8B, colored curves). We applied it to a selection of the modified candidate structures to show the difference in partitioning free energy between NAO representations with replaced bead types (Fig. 8B(b)).

The reaction coordinate was the normal of the membrane midplane and the PMF describes how the free energy of a compound changes as a function of the normal distance z between its center of mass and the membrane midplane. The reaction coordinate was split into 24 individual sampling windows and the molecule was kept close to the center z_i of each window i along the reaction coordinate z by a biasing

950 | *RSC Chem. Biol.*, 2022, **3**, 941–954

© 2022 The Author(s). Published by the Royal Society of Chemistry

potential of 1000 kJ mol^{-1} nm^{-2}. Unbiased potentials of mean force were extracted from the biased Umbrella simulations by means of the weighted histogram analysis method[89–91] and the corresponding errors *via* bootstrapping.[92]

Virtual screening

Molecules were selected from the MCULE database of purchasable, in-stock compounds (**https://mcule.com/**, version 18-08-17,[58] (Fig. 8C)). This was done using Morgan circular fingerprints[93] implemented in the RDKit[62] with feature-based atom invariants and a bit vector length of 2084 bits. The interaction radius was set to two, considering the two nearest neighbors of each atom, the setting best suited for comparing diverse structures for similarity.[94] The chemical features defined in the RDKit for feature-based circular fingerprints (FCFP) are hydrogen bond donor and acceptor sites, aromaticity, the presence of a halogen and acidic or basic properties. The resulting FCFP representations of the molecules were used to calculate the Tanimoto similarity coefficient[95] to the FCFP representation of NAO. The similarity score reads as follows: 0.0 ≡ no similarity at all to 1.0 ≡ identity.

Liposome preparation

For liposome preparation, the lipid or lipid mixture of interest (dissolved in chloroform) was mixed with Laurdan (dissolved in methanol) in a 500 : 1 molar ratio. If needed, a substance (dissolved in methanol) was added at the indicated concentration. The solvents were removed under a gentle nitrogen stream and vacuum desiccation overnight. The next day, 300 μL of 10 mM 4-(2-hydroxyethyl)-1-piperazineethanesulfonic acid (HEPES)-buffer (pH 7.4, 150 mM NaCl) was added and the lipid film was rehydrated, resulting in a solution with 300 μM total lipid. The mixture was vortexed two times for 1 minute. To prepare large unilamellar liposomes (LUVs), five freeze–thaw cycles were performed.

Laurdan fluorescence spectroscopy and generalized polarization (GP) values

Laurdan spectra were recorded at 25 °C using a Jasco Spectrofluorometer FP-8500 (Jasco Deutschland GmbH, Pfungstadt, GER). The excitation and emission band widths were set to 2.5 nm. Upon excitation at 360 nm, spectra were recorded from 400 to 600 nm. Each lipid composition was measured at least three times using freshly prepared liposomes. Generalized polarization (GP) values were calculated from the fluorescence emission spectra using the following equation:[96]

$$GP = \frac{I_{440} - I_{490}}{I_{440} + I_{490}} \qquad (5)$$

I_{440} and I_{490} are the emission intensities at 440 and 490 nm, respectively. For easier comparison, the ΔGP value was calculated using mean GP values determined in presence (+SM$_{XX}$) or absence (−SM$_{XX}$) of the small molecules with the following equation.

$$\Delta GP = GP_{+SM_{xx}} - GP_{-SM_{xx}} \qquad (6)$$

$_{XX}$ is a number between 1 and 22.

For each mean value, the standard error of the mean (SEM) was calculated, and the error for ΔGP and ΔGP_CL/ΔGP_PG (Fig. S3, ESI†) was calculated based on Gaussian error propagation.

Fluorescence measurements using the emission of SM$_{19}$

LUVs containing different amounts of 1,2-dioleoyl-*sn*-glycero-3-phosphocholine (DOPC) and 1,2-dioleoyl-*sn*-glycero-3-phosphoglycerol (DOPG) or cardiolipin (CL, 1,3-bis[1,2-dioleoyl-*sn*-glycero-3-phospho]-glycerol (TOCL)), respectively, were prepared as described. 3 μM SM$_{19}$ (2-[(*E*)-2-[4-(dimethylamino)phenyl]ethenyl]-3-ethyl-1,3-benzothiazol-3-ium iodide) was mixed with the lipids during liposome preparation. Fluorescence spectra were measured using a Jasco Spectrofluorometer FP-8500 (Jasco Deutschland GmbH, Pfungstadt, GER). The sample was excited at 500 nm and spectra were recorded from 520 to 680 nm. The band widths were set to 2.5 nm.

Fluorescence measurements of SM$_{19}$ in presence of *E. coli*

Escherichia coli strain MC4100 was grown in terrific broth (TB)-medium buffered with 10% K$_2$HPO$_4$/KH$_2$PO$_4$ (0.17 M/0.72 M). From an overnight culture, containing 10 mL TB medium with 1 : 1000 streptomycin (50 mg mL^{-1}), *E. coli* MC4100 were pelleted. The cells were washed three times with 10 mM HEPES buffer (pH 7.4, 150 mM NaCl) and resuspended in buffer to a final OD$_{600}$ of 2. Different concentrations of SM$_{19}$ (dissolved in water) were added to 500 μL of cells and incubated for 5 minutes. The emission spectra of SM$_{19}$ were recorded between 520 and 680 nm with a Jasco Spectrofluorometer FP-8500 (Jasco Deutschland GmbH, Pfungstadt, GER), upon excitation at 500 nm. The intensity at 592 nm was plotted.

Oxygen consumption of *E. coli*

For *E. coli* oxygen consumption measurements, a PreSens Fibox 3 Minisensor and an Oxygen Sensitive Optrode (DP-PSt3-L2.5-5510-YOP, PreSens Precision Sensing GmbH, Regensburg, Germany) was used. *E. coli* MC4100 cells from an overnight culture (prepared as described above) were diluted and grown until an OD$_{600}$ of around 0.6 was reached. The cells were harvested, and the pellet was resuspended in 200 μL PBS Puffer (137 mM NaCl, 2.7 mM KCl, 12 mM H$_3$PO$_4$, pH = 7.4) containing 10 mM EDTA. Upon incubation for 5 minutes, cells were pelleted and resuspended in TB media (OD$_{600}$ = 0.2). SM$_{19}$ was added up to a final concentration of 10 μM. 3 mL cells were placed in the reaction chamber, the chamber was closed airtight and the measurement was started at 37 °C. The measurement was stopped when the oxygen amount reached 0 μmol L^{-1}.

Generation and cultivation of *P. anserina* strains

The wild-type strain "s"[97] and the ΔPaCrd1-mutant[16] of *P. anserina* was used in this study. The ΔPaCrd1-mutant lacking the gene encoding PaCRD1 (UniProt B2AX19) was generated as described in ref. 16. Monokaryotic ascospores were allowed to germinate at BMM medium containing 80 mM ammonium acetate for 2 days at 27 °C in the dark. For mitochondria isolation, monokaryotic strains of wild-type and ΔPaCrd1 were

© 2022 The Author(s). Published by the Royal Society of Chemistry

RSC Chem. Biol., 2022, **3**, 941–954 | 951

grown on cellophane foil covered solid M2 agar under constant light for 2 days at 27 °C. After 2 days, grown mycelia were transferred to CM for 2 days at 27 °C with shaking.[98]

Isolation of mitochondria from *P. anserina*

Isolation of mitochondria was performed as described in.[98] Briefly, grown mycelia of 6 days old strains were disrupted in isotonic mitochondria buffer with 0.2% (w/v) of bovine serum albumin (BSA) (Sigma-Aldrich, St. Louis, Missouri, USA, A6003). The homogenate was filtered through nettle cloth and centrifuged at 600*g* for 10 min at 4 °C. Subsequently, the supernatant was filtered through glass wool and centrifuged at 12 000*g* for 20 min at 4 °C. The pellet was resuspended in isotonic mitochondrial buffer without BSA and centrifuged at 15 000*g* for 20 min at 4 °C. The mitochondria were enriched in the exterior circle of the pellet. The interior part (consisting of vacuoles) was removed, and the mitochondria were resuspended in isotonic mitochondrial buffer without BSA. The freshly isolated mitochondria were immediately used for respirometry.

Respirometry of *P. anserina* mitochondria

For measurement of the mitochondrial oxygen consumption rate, 150 µg of freshly isolated mitochondria was used and measured by high-resolution respirometry at 27 °C (Oxygraph-2k series C and G, OROBOROS Instruments, Innsbruck, Austria). Mitochondria were injected into a chamber with 2 ml of air-saturated buffer (0.3 M sucrose, 10 mM KH_2PO_4, 5 mM $MgCl_2$, 1 mM EGTA, 10 mM KCl and 0.1% BSA; pH 7.2) in presence *vs.* absence of 1 µM SM_{19}. To stimulate complex I-dependent phosphorylating respiration in the presence of ADP, 10 mM pyruvate (Sigma-Aldrich, P2256), 2 mM malate (Sigma-Aldrich, M1000) and 1.5 mM ADP (Sigma-Aldrich, A5285) was added.[99] When oxygen consumption reached a constant level, 1 mM potassium cyanide (KCN, inhibitor of cytochrome *c* oxidase (COX)) and 1 mM salicylhydroxamic acid (SHAM, inhibitor of the alternative oxidase (AOX)) were added to completely block respiration. Wild-type and *ΔPaCrd1* mitochondria were analyzed in presence of absence of 1 µM SM_{19}. For analyzing the data, the manufacturer's software DatLab 6 was used.

Author contributions

Conceptualization: T. B., H. D. O. and D. S.; methodology: I. K., B. M. and A. J.; software: B. M. and T. B.; validation: I. K., B. M., A. J., N. H., T. B., H. D. O. and D. S.; formal analysis: I. K., N. H., A. J. and B. M.; investigation: I. K., A. J. and B. M.; resources: T. B., H. O., D. S.; data curation: H. D. O., T. B. and D. S.; writing – original draft: I. K., A. J., B. M.; writing – review & editing: N. H., T. B., H. D. O., D. S.; visualization: I. K., A. J., B. M.; supervision: T. B., H. D. O., D. S.; project administration: D. S., T. B., H. D. O.; funding acquisition: T. B., H. D. O. and D. S.

Conflicts of interest

There are no conflicts to declare.

Acknowledgements

References

1 T. Harayama and H. Riezman, *Nat. Rev. Mol. Cell Biol.*, 2018, **19**, 281–296.

2 G. Van Meer, D. R. Voelker and G. W. Feigenson, *Nat. Rev. Mol. Cell Biol.*, 2009, **101**, 1–4.

3 J. M. Berg, J. L. Tymoczko and L. Stryer, *Stryer Biochemie*, Springer Berlin Heidelberg, Berlin, Heidelberg, 7th edn, 2013.

4 G. Paradies, V. Paradies, F. M. Ruggiero and G. Petrosillo, *Cells*, 2019, **8**, 728.

5 I. Barák and K. Muchová, *Int. J. Mol. Sci.*, 2013, **14**, 4050–4065.

6 E. R. Moellering and C. Benning, *Trends Plant Sci.*, 2011, **16**, 98–107.

7 M. C. Pangborn, *J. Biol. Chem.*, 1942, **143**, 247–256.

8 J. Dudek, *Front. Cell Dev. Biol.*, 2017, **5**, 1–17.

9 M. Schlame, M. Ren, Y. Xu, M. L. Greenberg and I. Haller, *Chem. Phys. Lipids*, 2005, **138**, 38–49.

10 L. E. Stefanyk, N. Coverdale, B. D. Roy, S. J. Peters and P. J. LeBlanc, *J. Membr. Biol.*, 2010, **234**, 207–215.

11 M. Schlame and M. L. Greenberg, *Biochim. Biophys. Acta, Mol. Cell Biol. Lipids*, 2017, **1862**, 3–7.

12 A. I. P. de Kroon, D. Dolis, A. Mayer, R. Lill and B. de Kruijff, *Biochim. Biophys. Acta, Biomembr.*, 1997, **1325**, 108–116.

13 G. Hallermayer and W. Neupert, *Biol. Chem.*, 1974, **355**, 279–288.

14 S. C. Kushwaha, M. Kates, J. K. G. Kramer and R. E. Subden, *Lipids*, 1976, **11**, 778–780.

15 E. Gryz, U. Perlińska-Lenart, K. Gawarecka, A. Jozwiak, S. Piłsyk, A. Lipko, M. Jemiola-Rzeminska, P. Bernat, A. Muszewska, K. Steczkiewicz, K. Ginalski, J. Długoński, K. Strzalka, E. Swiezewska and J. S. Kruszewska, *Int. J. Mol. Sci.*, 2019, **20**, 3043.

16 T. Löser, A. Joppe, A. Hamann and H. D. Osiewacz, *Cells*, 2021, **10**, 2775.

17 J. LeCocq and C. E. Ballou, *Biochemistry*, 1964, **3**, 976–980.

18 E. E. Kooijman, L. A. Swim, Z. T. Graber, Y. Y. Tyurina, H. Bayır and V. E. Kagan, *Biochim. Biophys. Acta, Biomembr.*, 2017, **1859**, 61–68.

19 R. H. Houtkooper and F. M. Vaz, *Cell. Mol. Life Sci.*, 2008, **65**, 2493–2506.

20 E. Kraffe, P. Soudant, Y. Marty, N. Kervarec and P. Jehan, *Lipids*, 2002, **37**, 507–514.

21 P. M. Oliver, J. A. Crooks, M. Leidl, E. J. Yoon, A. Saghatelian and D. B. Weibel, *J. Bacteriol.*, 2014, **196**, 3386–3398.

22 K. C. Huang, R. Mukhopadhyay and N. S. Wingreen, *PLoS Comput. Biol.*, 2006, **2**, e151.

23 A. J. Chicco and G. C. Sparagna, *Am. J. Physiol.*, 2007, **292**, C33–C44.

24 Z. Beleznai and V. Jancsik, *Biochem. Biophys. Res. Commun.*, 1989, **159**, 132–139.

25 F. Bisaccia and F. Palmieri, *Biochim. Biophys. Acta, Bioenerg.*, 1984, **766**, 386–394.

26 M. Müller, R. Moser, D. Cheneval and E. Carafoli, *J. Biol. Chem.*, 1985, **260**, 3839–3843.

27 V. E. Kagan, Y. Y. Tyurina, H. Bayir, C. T. Chu, A. A. Kapralov, I. I. Vlasova, N. A. Belikova, V. A. Tyurin, A. Amoscato, M. Epperly, J. Greenberger, S. DeKosky, A. A. Shvedova and J. Jiang, *Chem. – Biol. Interact.*, 2006, **163**, 15–28.

28 F. Gonzalvez and E. Gottlieb, *Apoptosis*, 2007, **12**, 877–885.

29 B. A. Wilson, A. Ramanathan and C. F. Lopez, *Biophys. J.*, 2019, **117**, 429–444.

30 T. Zhang, J. K. Muraih, N. Tishbi, J. Herskowitz, R. L. Victor, J. Silverman, S. Uwumarenogie, S. D. Taylor, M. Palmer and E. Mintzer, *J. Biol. Chem.*, 2014, **289**, 11584–11591.

31 C. W. T. Leung, Y. Hong, J. Hanske, E. Zhao, S. Chen, E. V. Pletneva and B. Z. Tang, *Anal. Chem.*, 2014, **86**, 1263–1268.

32 K. Pyrshev, S. Yesylevskyy and M. Bogdanov, *Biophys. J.*, 2021, **120**, 3776–3786.

33 H. H. Szeto, *Br. J. Pharmacol.*, 2014, **171**, 2029–2050.

34 A. Maftah, J. M. Petit and R. Julien, *FEBS Lett.*, 1990, **260**, 236–240.

35 A. Maftah, J. M. Petit, M.-H. Ratinaud and R. Julien, *Biochem. Biophys. Res. Commun.*, 1989, **164**, 185–190.

36 M. Septinus, T. Berthold, A. Naujok and H. W. Zimmermann, *Histochemistry*, 1985, **82**, 51–66.

37 M. H. Ratinaud, P. Leprat and R. Julien, *Cytometry*, 1988, **9**, 206–212.

38 J.-M. Petit, A. Maftah, M.-H. Ratinaud and R. Julien, *Eur. J. Biochem.*, 1992, **209**, 267–273.

39 P. F. Gallet, A. Maftah, J.-M. Petit, M. Denis-Gay and R. Julien, *Eur. J. Biochem.*, 1995, **228**, 113–119.

40 V. M. Gohil, J. Gvozdenovic-Jeremic, M. Schlame and M. L. Greenberg, *Anal. Biochem.*, 2005, **343**, 350–352.

41 J. D. Durrant and J. A. McCammon, *BMC Biol.*, 2011, **9**, 71.

42 T. Bereau, D. Andrienko and K. Kremer, *APL Mater.*, 2016, **4**, 053101.

43 S. Curtarolo, G. L. W. Hart, M. Buongiorno Nardelli, N. Mingo, S. Sanvito and O. Levy, *Nat. Mater.*, 2013, **12**, 191–201.

44 W. G. Noid, *J. Chem. Phys.*, 2013, **139**, 090901.

45 R. Menichetti, K. H. Kanekal and T. Bereau, *ACS Cent. Sci.*, 2019, **5**, 290–298.

46 D. Mohammadyani, N. Yanamala, A. K. Samhan-Arias, A. A. Kapralov, G. Stepanov, N. Nuar, J. Planas-Iglesias, N. Sanghera, V. E. Kagan and J. Klein-Seetharaman, *Biochim. Biophys. Acta, Biomembr.*, 2018, **1860**, 1057–1068.

47 K. J. Boyd, N. N. Alder and E. R. May, *Biophys. J.*, 2018, **114**, 2116–2127.

48 B. Mohr, K. Shmilovich, I. Kleinwächter, D. Schneider, A. L. Ferguson and T. Bereau, *Chem. Sci.*, 2022, **13**, 4498.

49 L. A. Luévano-Martínez, M. F. Forni, V. T. dos Santos, N. C. Souza-Pinto and A. J. Kowaltowski, *Biochim. Biophys. Acta, Bioenerg.*, 2015, **1847**, 587–598.

50 E. Mileykovskaya, W. Dowhan, R. L. Birke, D. Zheng, L. Lutterodt and T. H. Haines, *FEBS Lett.*, 2001, **507**, 187–190.

51 J. D. Chodera, D. L. Mobley, M. R. Shirts, R. W. Dixon, K. Branson and V. S. Pande, *Curr. Opin. Struct. Biol.*, 2011, **21**, 150–160.

52 T. P. Straatsma, Free Energy by Molecular Simulation, in *Reviews in Computational Chemistry*, ed. K. B. Lipkowitz and D. B. Boyd, Wiley, 1996, vol. 9, DOI: [10.1002/9780470125861.ch2](https://doi.org/10.1002/9780470125861.ch2).

53 P. Kollman, *Chem. Rev.*, 1993, **93**, 2395–2417.

54 G. M. Torrie and J. Valleau, *J. Comput. Phys.*, 1977, **23**, 187–199.

55 J. Kästner, *Wiley Interdiscip. Rev.: Comput. Mol. Sci.*, 2011, **1**, 932–942.

56 S. J. Marrink, H. J. Risselada, S. Yefimov, D. P. Tieleman and A. H. de Vries, *J. Phys. Chem. B*, 2007, **111**, 7812–7824.

57 J. Planas-Iglesias, H. Dwarakanath, D. Mohammadyani, N. Yanamala, V. E. Kagan and J. Klein-Seetharaman, *Biophys. J.*, 2015, **109**, 1282–1294.

58 R. Kiss, M. Sandor and F. A. Szalai, *J. Cheminf.*, 2012, **4**, P17.

59 T. T. Tanimoto, *An elementary mathematical theory of classification and prediction*, International Business Machines Corp., 1985.

60 P. Jaccard, *New Phytol.*, 1912, **11**, 37–50.

61 A.-R. Nekoei and M. Vatanparast, *Phys. Chem. Chem. Phys.*, 2019, **21**, 623–630.

62 G. Landrum, RDKit: Open-Source Cheminformatics Software, https://www.rdkit.org, accessed 14 July 2021.

63 I. S. Kleinwächter, S. Pannwitt, A. Centi, N. Hellmann, E. Thines, T. Bereau and D. Schneider, *Membranes*, 2021, **11**, 254.

64 J. Seelig, *Biochim. Biophys. Acta, Biomembr.*, 2004, **1666**, 40–50.

65 T. Parasassi, G. De Stasio, G. Ravagnan, R. M. Rusch and E. Gratton, *Biophys. J.*, 1991, **60**, 179–189.

66 T. Parasassi, M. Di Stefano, M. Loiero, G. Ravagnan and E. Gratton, *Biophys. J.*, 1994, **66**, 120–132.

67 R. Gredilla, J. Grief and H. D. Osiewacz, *Exp. Gerontol.*, 2006, **41**, 439–447.

68 G. Oemer, J. Koch, Y. Wohlfarter, M. T. Alam, K. Lackner, S. Sailer, L. Neumann, H. H. Lindner, K. Watschinger, M. Haltmeier, E. R. Werner, J. Zschocke and M. A. Keller, *Cell Rep.*, 2020, **30**, 4281.e4–4291.e4.

69 T. Romantsov, Z. Guan and J. M. Wood, *Biochim. Biophys. Acta, Biomembr.*, 2009, **1788**, 2092–2100.

70 M. Schlame, S. Brody and K. Y. Hostetler, *Eur. J. Biochem.*, 1993, **212**, 727–733.

© 2022 The Author(s). Published by the Royal Society of Chemistry

RSC Chem. Biol., 2022, **3**, 941–954 | **953**

71 E. R. Pennington, K. Funai, D. A. Brown and S. R. Shaikh, *Biochim. Biophys. Acta, Mol. Cell Biol. Lipids*, 2019, **1864**, 1039–1052.

72 C. Sohlenkamp and O. Geiger, *FEMS Microbiol. Rev.*, 2015, **40**, 133–159.

73 X. Periole and S.-J. Marrink, *Methods in Molecular Biology*, 2013, pp. 533–565.

74 M. Dahlberg, *J. Phys. Chem. B*, 2007, **111**, 7194–7200.

75 M. Dahlberg and A. Maliniak, *J. Phys. Chem. B*, 2008, **112**, 11655–11663.

76 M. Dahlberg and A. Maliniak, *J. Chem. Theory Comput.*, 2010, **6**, 1638–1649.

77 S. Jo, X. Cheng, J. Lee, S. Kim, S. Park, D. S. Patel, A. H. Beaven, K. Il Lee, H. Rui, S. Park, H. S. Lee, B. Roux, A. D. MacKerell, J. B. Klauda, Y. Qi and W. Im, *J. Comput. Chem.*, 2017, **38**, 1114–1124.

78 S. O. Yesylevskyy, L. V. Schäfer, D. Sengupta and S. J. Marrink, *PLoS Comput. Biol.*, 2010, **6**, e1000810.

79 T. Bereau and K. Kremer, *J. Chem. Theory Comput.*, 2015, **11**, 2783–2791.

80 M. J. Abraham, T. Murtola, R. Schulz, S. Páll, J. C. Smith, B. Hess and E. Lindahl, *SoftwareX*, 2015, **1–2**, 19–25.

81 G. Bussi, D. Donadio and M. Parrinello, *J. Chem. Phys.*, 2007, **126**, 014101.

82 M. Parrinello and A. Rahman, *J. Appl. Phys.*, 1981, **52**, 7182–7190.

83 T. Darden, D. York and L. Pedersen, *J. Chem. Phys.*, 1993, **98**, 10089–10092.

84 D. H. de Jong, S. Baoukina, H. I. Ingólfsson and S. J. Marrink, *Comput. Phys. Commun.*, 2016, **199**, 1–7.

85 W. Chen, Y. Deng, E. Russell, Y. Wu, R. Abel and L. Wang, *J. Chem. Theory Comput.*, 2018, **14**, 6346–6358.

86 A. Pohorille, C. Jarzynski and C. Chipot, *J. Phys. Chem. B*, 2010, **114**, 10235–10253.

87 P. V. Klimovich, M. R. Shirts and D. L. Mobley, *J. Comput. – Aided Mol. Des.*, 2015, **29**, 397–411.

88 M. R. Shirts and J. D. Chodera, *J. Chem. Phys.*, 2008, **129**, 124105.

89 S. Kumar, J. M. Rosenberg, D. Bouzida, R. H. Swendsen and P. A. Kollman, *J. Comput. Chem.*, 1992, **13**, 1011–1021.

90 T. Bereau and R. H. Swendsen, *J. Comput. Phys.*, 2009, **228**, 6119–6129.

91 J. S. Hub, B. L. de Groot and D. van der Spoel, *J. Chem. Theory Comput.*, 2010, **6**, 3713–3720.

92 T. F. Liao, C. Z. Mooney, R. D. Duval and S. R. Eliason, *Contemp. Sociol.*, 1995, **24**, 269.

93 D. Rogers and M. Hahn, *J. Chem. Inf. Model.*, 2010, **50**, 742–754.

94 P. Baldi and R. Nasr, *J. Chem. Inf. Model.*, 2010, **50**, 1205–1222.

95 D. Bajusz, A. Rácz and K. Héberger, *J. Cheminf.*, 2015, **7**, 20.

96 T. Parasassi, G. De Stasio, A. D'Ubaldo and E. Gratton, *Biophys. J.*, 1990, **57**, 1179–1186.

97 G. Rizet, *C. R. Hebd. Seances Acad. Sci.*, 1953, **237**, 838–840.

98 H. D. Osiewacz, A. Hamann and S. Zintel, *Methods in Molecular Biology*, 2013, vol. 965, pp. 439–462.

99 V. Warnsmann, S. Hainbuch and H. D. Osiewacz, *Front. Genet.*, 2018, **9**, 1–14.